

## **Supporting Information**

# **Long-Term Stable Lithium Metal Anode in Highly Concentrated Sulfolane-Based Electrolytes with Ultrafine Porous Polyimide Separator**

Yuta Maeyoshi<sup>a,\*</sup>, Dong Ding<sup>a</sup>, Masaaki Kubota<sup>a</sup>, Hiroshi Ueda<sup>b</sup>, Koji Abe<sup>c</sup>, Kiyoshi Kanamura<sup>a,b,d</sup>, Hidetoshi Abe<sup>a,\*</sup>

<sup>a</sup>ABRI Co., Ltd., Building P-302, Tokyo Metropolitan University, 1-1 Minami-Ohsawa, Hachioji, Tokyo 192-0397, Japan

<sup>b</sup>3DOM Inc., 3-9 Moriya-cho, Kanagawa-ku, Yokohama, Kanagawa 221-0022, Japan

<sup>c</sup>Division of Energy Materials Chemistry, Research Center for Advanced Science and Innovation, Organization for Research Initiatives, Yamaguchi University, 2-16-1 Tokiwadai, Ube, Yamaguchi 755-8611, Japan

<sup>d</sup>Department of Applied Chemistry for Environment, Graduate School of Urban Environmental Sciences, Tokyo Metropolitan University, 1-1 Minami-Ohsawa, Hachioji, Tokyo 192-0397, Japan

\*E-mail: y-maeyoshi@abri.co.jp

\*E-mail: h-abe@abri.co.jp

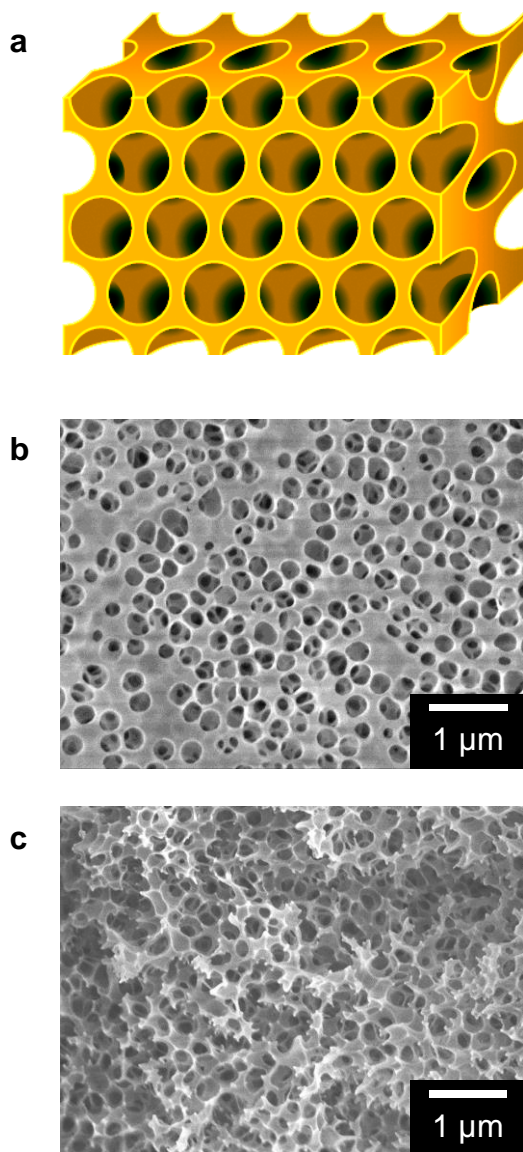


**Figure S1.** (a) Schematic of three-dimensionally ordered macroporous (3DOM) structure. SEM images of (b) surface and (c) cross-section of 3DOM PI separator.

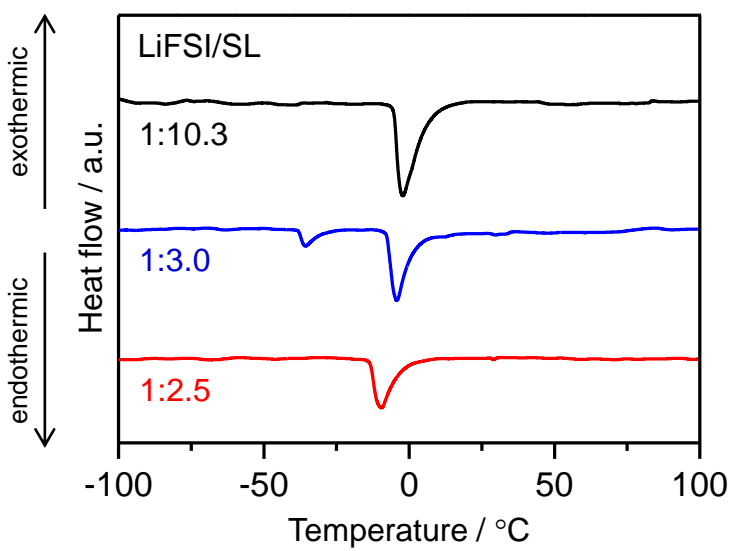


**Figure S2.** DSC thermograms of LiFSI/SL solutions at a rate of  $10\text{ }^{\circ}\text{C min}^{-1}$ .

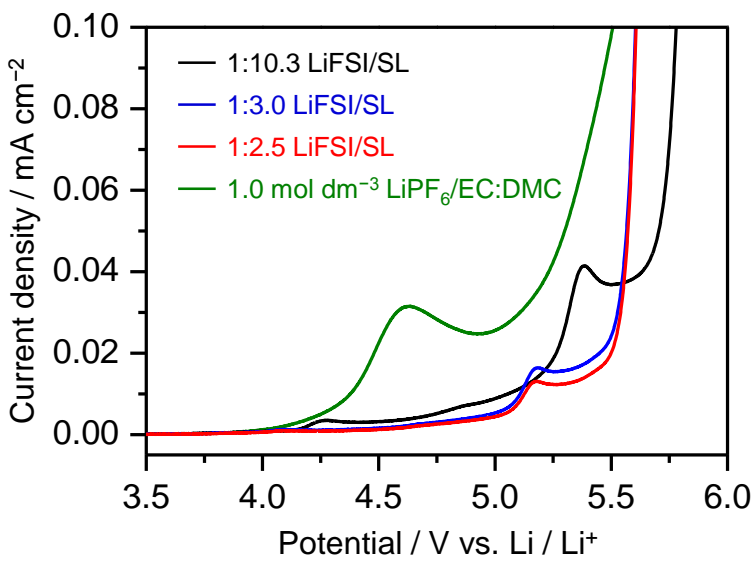


**Figure S3.** Linear sweep voltammograms of LiFSI/SL solutions and a conventional 1.0 mol dm<sup>-3</sup> LiPF<sub>6</sub>/EC:DMC electrolyte at a scan rate of 1 mV s<sup>-1</sup> at room temperature with three-electrode cell employing a platinum disk as a working electrode and Li foils as reference and counter electrodes.

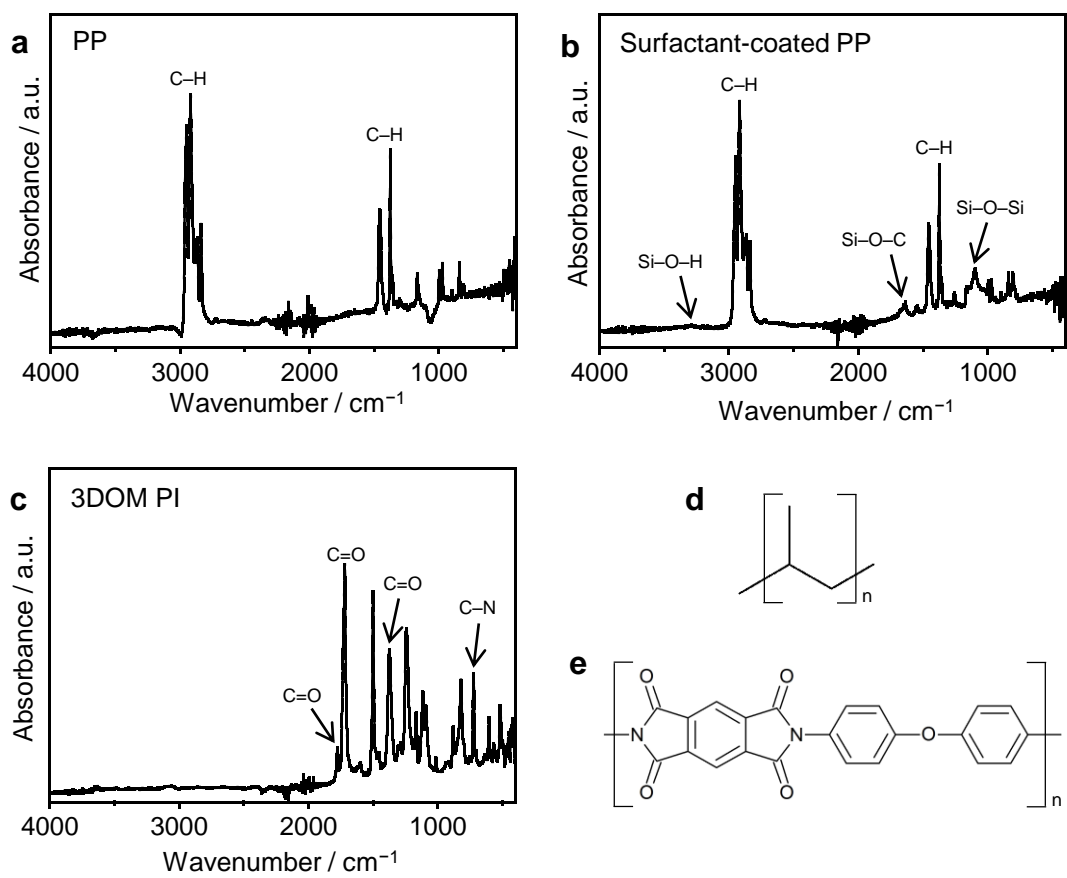


**Figure S4.** FT-IR spectra of (a) PP, (b) surfactant-coated PP, and (c) 3DOM PI separators. The peaks were assigned based on the previous reports.<sup>1,2</sup> Chemical structures of (d) PP and (e) PI.

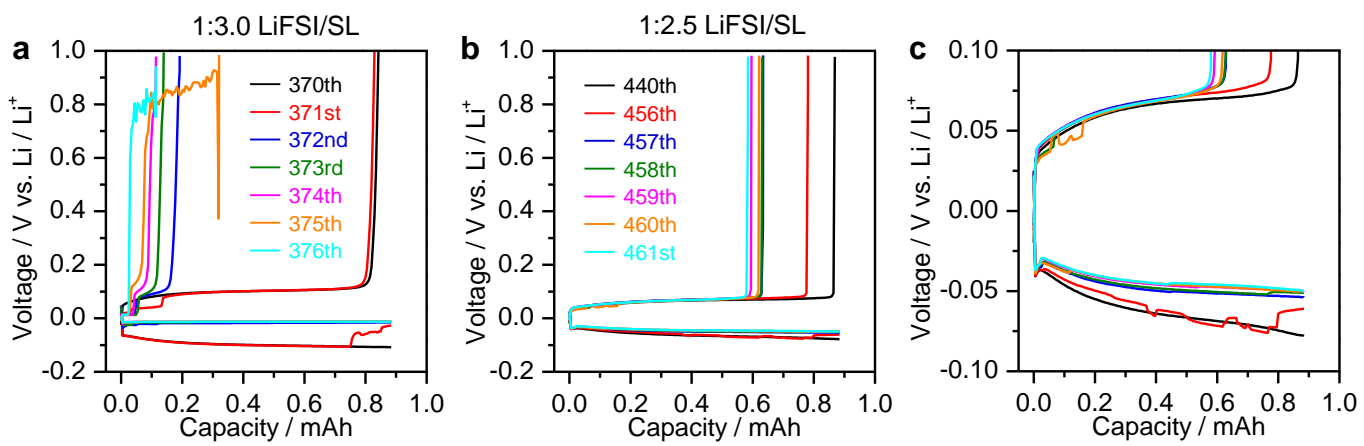


**Figure S5.** Voltage versus capacity of lithium plating/stripping in Cu|Li cells using LiFSI/SL solutions with salt-to-solvent molar ratios of (a) 1:3.0 and (b) 1:2.5 after long-term cycling at 30 °C. A current density and a deposition capacity are 1.0 mA cm<sup>-2</sup> and 0.5 mAh cm<sup>-2</sup>, respectively. (c) The magnified view of b.

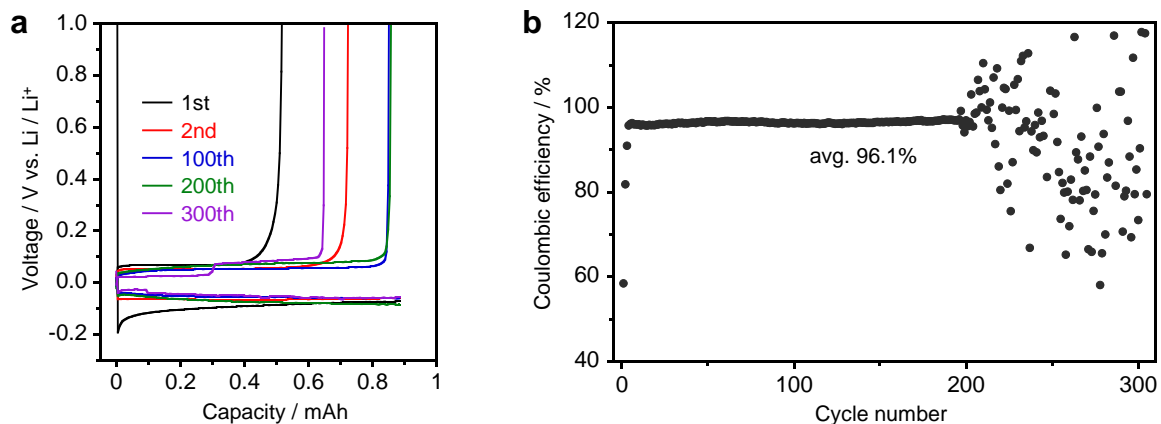


**Figure S6.** (a) Voltage versus capacity and (b) Coulombic efficiency versus cycle number of lithium plating/stripping in Cu|Li cells using surfactant-coated PP separator and 1:2.5 LiFSI/SL solution at 30 °C. A current density and a deposition capacity are 1.0 mA cm<sup>-2</sup> and 0.5 mAh cm<sup>-2</sup>, respectively.

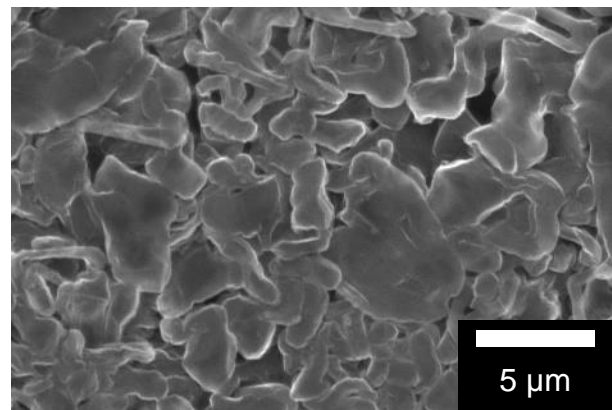


**Figure S7.** SEM image of morphology of lithium metal deposited on Cu foil in LiFSI/SL solution with a salt-to-solvent molar ratio of 1:2.5 using surfactant-coated PP separator at 30 °C. A current density and a deposition capacity are 1.0 mA cm<sup>-2</sup> and 1.0 mAh cm<sup>-2</sup>, respectively.

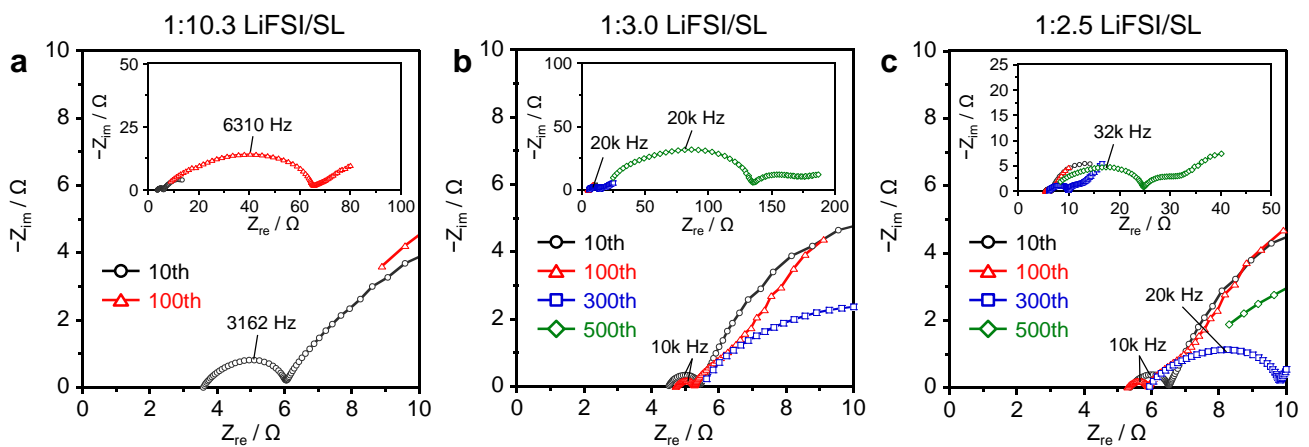


**Figure S8.** Nyquist plots of EIS measurements for Li|Li cells using LiFSI/SL solutions with salt-to-solvent molar ratios of (a) 1:10.3, (b) 1:3.0, and (c) 1:2.5. The cells were measured at 30 °C after 10, 100, 300, and 500 lithium plating/stripping cycles. The insets are magnified views of each figure.

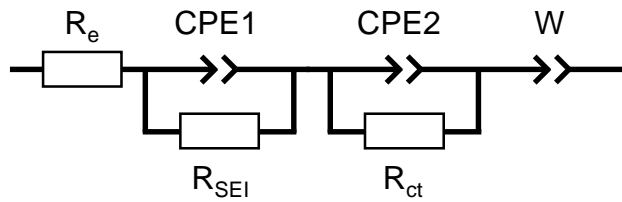


**Figure S9.** Equivalent circuit model established for fitting of the EIS spectra in Figure S8. The model is composed of the bulk electrolyte resistance ( $R_e$ ), the SEI resistance ( $R_{SEI}$ ) and the charge-transfer resistance of lithium metal ( $R_{ct}$ ), the constant phase elements (CPE1 and CPE2) associated with the double layer capacitance between the electrode and electrolyte, and the Warburg impedance (W) associated with diffusion of lithium-ion.<sup>3,4</sup>

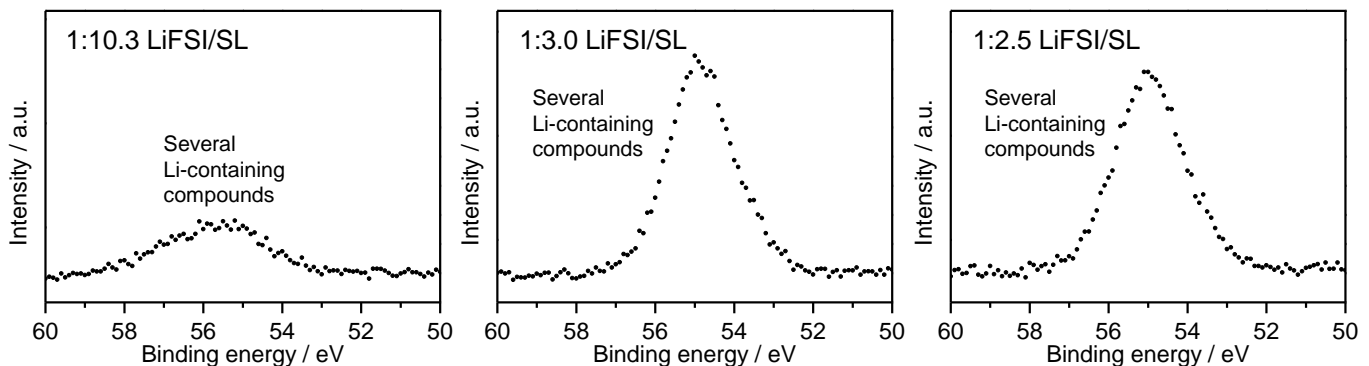


**Figure S10.** High-resolution Li 1s spectra of the SEI layers on Li foils after 50 plating/stripping cycles in LiFSI/SL solutions with salt-to-solvent molar ratios of 1:10.3, 1:3.0, and 1:2.5. In the spectra, various Li-containing compounds give a peak at almost the same binding energy in 53–56 eV and hence, no useful information was obtained.

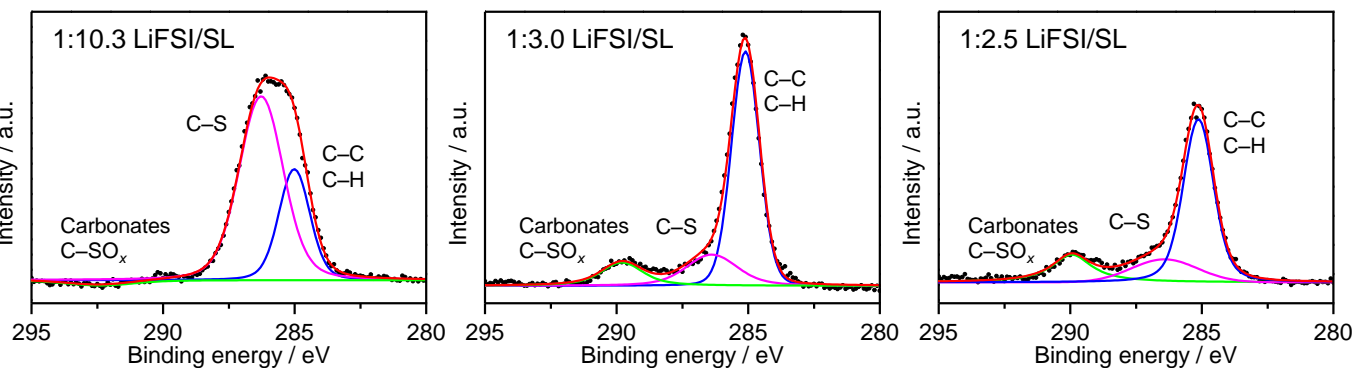


**Figure S11.** High-resolution C 1s spectra of the SEI layers on Li foils after 50 plating/stripping cycles in LiFSI/SL solutions with salt-to-solvent molar ratios of 1:10.3, 1:3.0, and 1:2.5. Dots and solid lines denote experimental spectra and fitting curves, respectively.

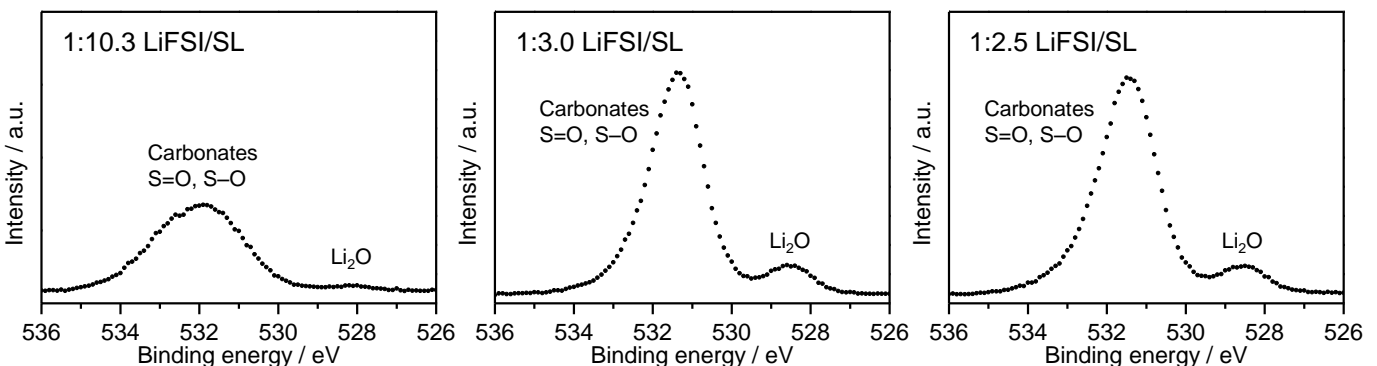


**Figure S12.** High-resolution O 1s spectra of the SEI layers on Li foils after 50 plating/stripping cycles in LiFSI/SL solutions with salt-to-solvent molar ratios of 1:10.3, 1:3.0, and 1:2.5.

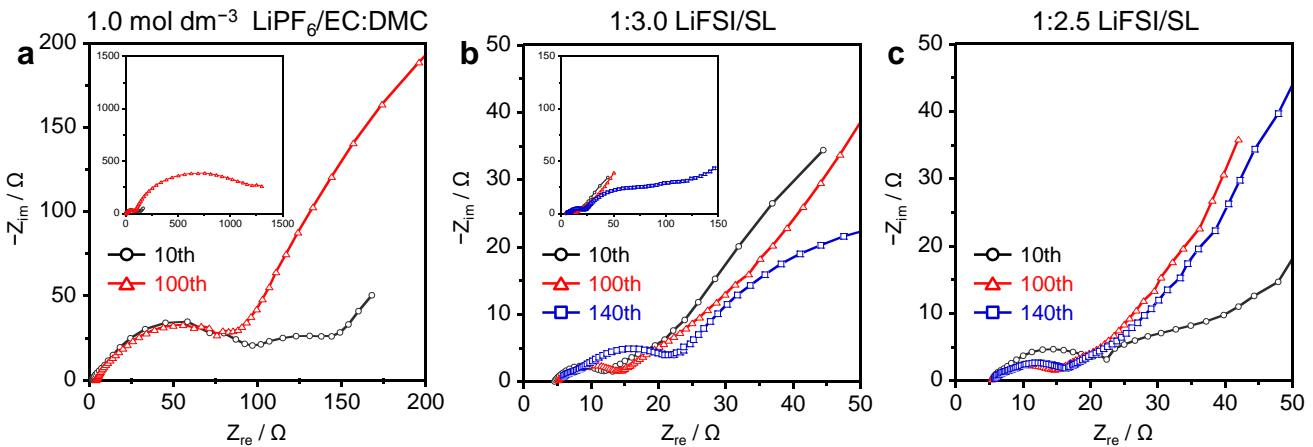


**Figure S13.** Nyquist plots of EIS measurements for LiFePO<sub>4</sub>|Li cells using (a) 1.0 mol dm<sup>-3</sup> LiPF<sub>6</sub>/EC:DMC (1:1 by volume) and LiFSI/SL solutions with salt-to-solvent molar ratios of (b) 1:3.0 and (c) 1:2.5. The cells were measured at 30 °C after 10, 100 and 140 cycles of the charge/discharge test.

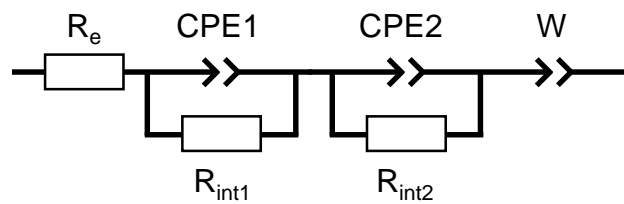


**Figure S14.** Equivalent circuit model established for fitting of the EIS spectra in Figure S13. The model is composed of the bulk electrolyte resistance ( $R_e$ ), the interfacial resistances ( $R_{int1}$  and  $R_{int2}$ ) of the lithium metal anode and LiFePO<sub>4</sub> cathode, the constant phase elements (CPE1 and CPE2) associated with the double layer capacitance between the electrodes and electrolyte, and the Warburg impedance (W) associated with diffusion of lithium-ion.<sup>5,6</sup>

**Table S1.** Electrolyte resistance ( $R_e$ ) and interfacial resistances ( $R_{int1}$  and  $R_{int2}$ ) based on the EIS measurements of  $\text{LiFePO}_4|\text{Li}$  cells using  $1.0 \text{ mol dm}^{-3}$   $\text{LiPF}_6/\text{EC:DMC}$  (1:1 by volume) and LiFSI/SL solutions with salt-to-solvent molar ratios of 1:3.0 and 1:2.5. The cells were measured after 10, 100, and 140 cycles of the charge/discharge test.

Electrolyte	Resistances after 10 cycles / $\Omega$			Resistances after 100 cycles / $\Omega$			Resistances after 140 cycles / $\Omega$		
	$R_e$	$R_{int1}$	$R_{int2}$	$R_e$	$R_{int1}$	$R_{int2}$	$R_e$	$R_{int1}$	$R_{int2}$
1.0 mol $\text{dm}^{-3}$ $\text{LiPF}_6/\text{EC:DMC}$	1.57	111	23.5	3.87	84.3	1210	-	-	-
1:3.0 LiFSI/SL	4.51	7.70	6.00	4.84	10.2	8.15	5.66	12.6	163
1:2.5 LiFSI/SL	5.18	16.6	18.0	4.90	10.9	7.01	5.24	11.8	18.8

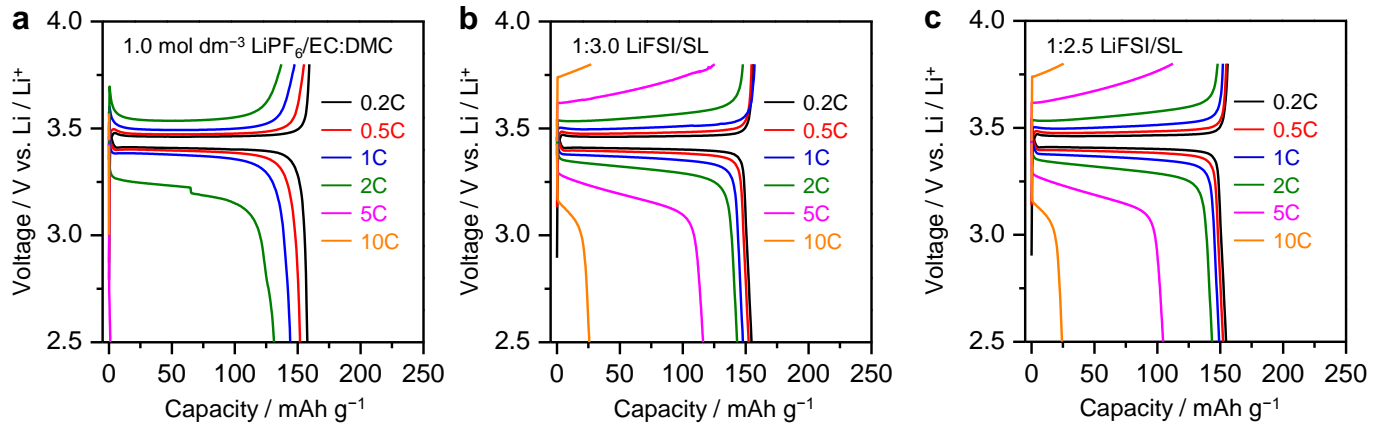


**Figure S15.** Charge/discharge curves for LiFePO<sub>4</sub>|Li cells using (a) 1.0 mol dm<sup>-3</sup> LiPF<sub>6</sub>/EC:DMC (1:1 by volume) and LiFSI/SL solutions with salt-to-solvent molar ratios of (b) 1:3.0 and (c) 1:2.5 at various C rates. Charge and discharge were conducted at the same C rate at 30 °C in a voltage range of 2.5–3.8 V.

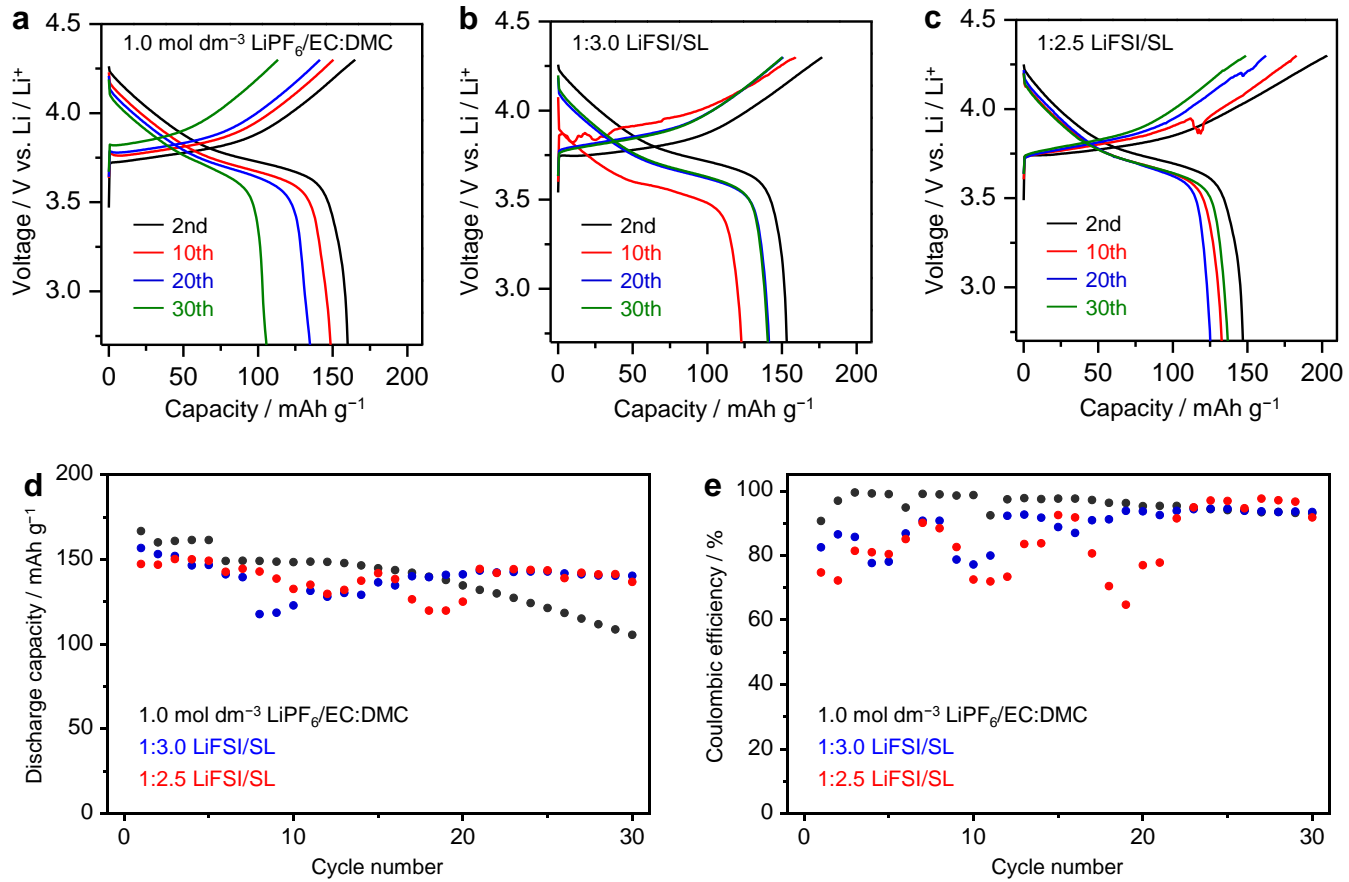


**Figure S16.** Charge/discharge curves for NCM523|Li cells using (a) 1.0 mol dm<sup>-3</sup> LiPF<sub>6</sub>/EC:DMC (1:1 by volume) and LiFSI/SL solutions with salt-to-solvent molar ratios of (b) 1:3.0 and (c) 1:2.5. The curves of 2nd, 10th, 20th, and 30th cycles are shown. (d) Discharge capacity and (e) Coulombic efficiency versus cycle number for the cells. The cycling tests were conducted at 0.5C rate after an initial one cycle at 0.1C rate and then four cycles at 0.2C rate at 30 °C in a voltage range of 2.7–4.3 V.

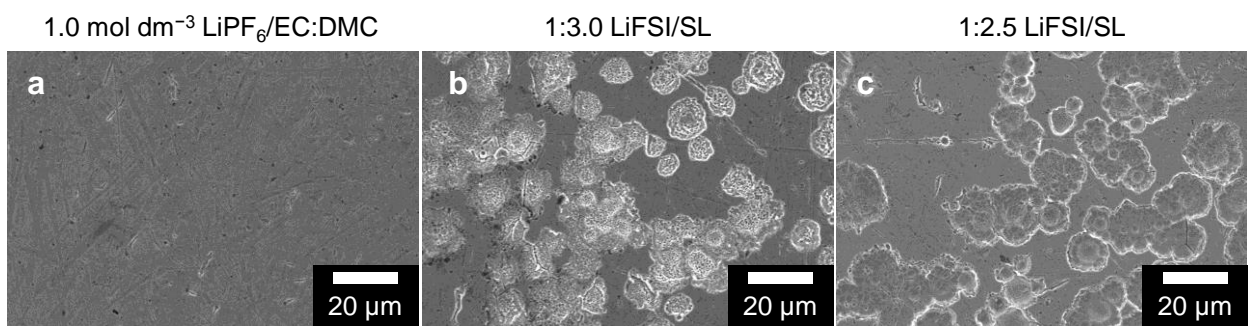


**Figure S17.** SEM images of stainless steel (SS316L) coin cell cases after 30 cycles of the charge/discharge tests in NCM523|Li cells using (a) 1.0 mol dm<sup>-3</sup> LiPF<sub>6</sub>/EC:DMC (1:1 by volume) and LiFSI/SL solutions with salt-to-solvent molar ratios of (b) 1:3.0 and (c) 1:2.5.

## REFERENCES

- (1) Li, X.; Tao, J.; Hu, D.; Engelhard, M. H.; Zhao, W.; Zhang, J. G.; Xu, W. Stability of Polymeric Separators in Lithium Metal Batteries in a Low Voltage Environment. *J. Mater. Chem. A* **2018**, *6*, 5006–5015.
- (2) Maeyoshi, Y.; Miyamoto, S.; Munakata, H.; Kanamura, K. Enhanced Cycle Stability of LiCoPO<sub>4</sub> by Using Three-Dimensionally Ordered Macroporous Polyimide Separator. *J. Power Sources* **2017**, *350*, 103–108.
- (3) Liu, W.; Lin, D.; Pei, A.; Cui, Y. Stabilizing Lithium Metal Anodes by Uniform Li-Ion Flux Distribution in Nanochannel Confinement. *J. Am. Chem. Soc.* **2016**, *138* (47), 15443–15450.
- (4) Girard, G. M. A.; Hilder, M.; Nucciarone, D.; Whitbread, K.; Zavorine, S.; Moser, M.; Forsyth, M.; MacFarlane, D. R.; Howlett, P. C. Role of Li Concentration and the SEI Layer in Enabling High Performance Li Metal Electrodes Using a Phosphonium Bis(Fluorosulfonyl)Imide Ionic Liquid. *J. Phys. Chem. C* **2017**, *121* (39), 21087–21095.
- (5) Fan, X.; Chen, L.; Borodin, O.; Ji, X.; Chen, J.; Hou, S.; Deng, T.; Zheng, J.; Yang, C.; Liou, S. C.; Amine, K.; Xu, K.; Wang, C. Non-Flammable Electrolyte Enables Li-Metal Batteries with Aggressive Cathode Chemistries. *Nat. Nanotechnol.* **2018**, *13*, 715–722.
- (6) Zheng, J.; Engelhard, M. H.; Mei, D.; Jiao, S.; Polzin, B. J.; Zhang, J. G.; Xu, W. Electrolyte Additive Enabled Fast Charging and Stable Cycling Lithium Metal Batteries. *Nat. Energy* **2017**, *2*, 17012.